Increasing both the electromagnetic shielding and thermal conductive properties of three-dimensional graphene-CNT-SiC hybrid materials

FENG Fan[1,2], HAN Zhi-dong[1,*], WEI Bing[3,*], WANG Yang[2], WANG Fei-zhou[2], JIAO Yan-yan[2], WANG Zhen-ting[3]

（1. *School of Materials Science and Chemical Engineering*, *Harbin University of Science and Technology*, *Harbin* 150081, *China*;
2. *Qitaihe Baotailong Graphene new materials Co.*, *LTD*, *Qitaihe* 154603, *China*;
3. *School of Materials Science and Engineering*, *Heilongjiang University of Science and Technology*, *Harbin* 150022, *China*）

Abstract: During the operation of electronic devices, a considerable amount of heat and electromagnetic radiation is emitted. Therefore, the investigation of materials with electromagnetic shielding and thermal management abilities has significant importance. Hybrid materials of three-dimensional graphene networks containing both carbon nanotubes (CNTs) and SiC whiskers (3D graphene-CNT-SiC) were synthesized. Using an aqueous-phase reduction method for the self-assembly of the graphene oxide, a three-dimensional porous graphene structure was fabricated. SiC whiskers, inserted between the graphene layers, formed a framework for longitudinal thermal conduction, while CNTs attached to the SiC surface, created a dendritic structure that increased the bonding between the SiC whiskers and graphene, improving dielectric loss and thermal conductivity. It was found that the thermal conductivity of the hybrid material reached 123 $W \cdot m^{-1} \cdot K^{-1}$, with a shielding effectiveness of 29.3 dB when the SiC addition was 2%. This result indicates that 3D graphene-CNT-SiC has excellent thermal conductivity and electromagnetic shielding performance.

Key words: Thermal management; Electromagnetic Shielding; 3D graphene; Silicon carbide; Carbon nanotubes

1 Introduction

Artificial intelligence (AI), exemplified by ChatGPT, has ushered in a new era of technological revolution, relying on high-performance chips and large-scale integrated circuits as fundamental hardware. However, the escalating integration and power density of these components present formidable challenges for heat dissipation[1–5]. Moreover, their operation emits considerable electromagnetic radiation, which disrupts neighboring devices and poses health risks. Hence, materials for electronic packaging with superior thermal conductivity and electromagnetic interference (EMI) shielding properties are highly desirable[6]. To expedite the advancement of AI, the creation of dual-functional electronic packaging materials possessing both high thermal conductivity and EMI shielding capabilities holds practical significance.

Graphene, a two-dimensional (2D) material, boasts remarkable properties such as high electrical and thermal conductivity, large specific surface area, and high electron mobility. Moreover, its unique electron polarization and defect polarization relaxation impart exceptional electromagnetic shielding capabilities[7–10]. Silicon carbide (SiC) exhibits outstanding thermal conductivity (reaching up to 490 $W \cdot m^{-1} \cdot K^{-1}$ theoretically), notable strength and thermal stability, making it widely used in the field of thermal management[11–14]. Leveraging the distinct advantages of graphene and SiC in electromagnetic shielding and thermal conduction, researchers have conducted extensive studies on their composites.

Shi et al.[15] introduced an innovative method that integrates ice templating with mechanical vibration to develop filler networks composed of reduced graphene oxide (rGO) and silicon carbide whiskers (SiC), arranged both horizontally and vertically. This compo-

Received date: 2024-05-29; **Revised date:** 2024-09-11
Corresponding author: HAN Zhi-dong, Professor. E-mail: zhidong.han@hrbust.edu.cn;
WEI Bing, Lecturer. E-mail: weibing@usth.edu.cn
Author introduction: FENG Fan, PhD candidate. E-mail: Fe19910830@163.com
Supplementary data associated with this article can be found in the online version.

site, containing 3.88% hybrid fillers, achieved a through-plane thermal conductivity of 5.24 $W \cdot m^{-1} \cdot K^{-1}$. The thermal conductivity anisotropy of the composite was measured at 1.35, which is attributed to the strategic orientation of the filler network in both vertical and horizontal planes. Furthermore, the composite exhibited a total electromagnetic interference (EMI) shielding effectiveness of 35.2 dB, coupled with low electromagnetic reflection, indicating excellent EMI shielding properties. Xie et al.[16] prepared surface-modified C/C composites using C/C composites as the matrix, 1D SiC as an intermediary layer, and vertically oriented graphene for modification. As a result, the specific surface area of the C/C composites was significantly enhanced, rising from 0.25 to 10.44 $m^2 \cdot g^{-1}$. This modification also led to an improvement in electromagnetic interference (EMI) shielding efficiency (SE), which increased from 13.08 to 23.86 dB. He et al.[17] fabricated SrGO/(C-SiC)$_n$ composite materials using RGO foam produced by depositing a carbon-reinforced layer, and alternating filling of pyrolytic carbon and SiC through the precursor infiltration and pyrolysis (PIP) technique. By increasing the number of alternating PIP cycles, significant improvements were observed in the mechanical, electrical, and EMI shielding properties of the SrGO/(C-SiC)*n* composites. The optimized composite material demonstrated remarkable performance across the X, Ku, K, and Ka bands over a wide bandwidth of 32 GHz, with an electrical conductivity of 8.52 $S \cdot cm^{-1}$ and an average EMI SE of 70.2 dB. This high EMI SE was attributed to substantial conduction loss within the highly conductive SrGO framework and polarization relaxation at the numerous heterogeneous PyC/SiC interfaces. Zhao et al.[18] designed a convenient approach for synthesizing SiC nanowires at the edges of RGO sheets to connect adjacent RGO sheets. This approach aims to reduce phonon scattering and enhance the thermal conductivity of graphene aerogels. Prior to this, chemically reduced RGO/Si aerogels with vertically aligned structures were created using a combination of chemical reduction and freeze-drying to improve their in-plane thermal conductivity. HGA-5 imparted EP composites (with 2.87% filler content) with an impressive in-plane thermal conductivity of 3.59 $W \cdot m^{-1} \cdot K^{-1}$. The optimal EMI shielding performance reached 38 dB.

While research on graphene/SiC composites for electromagnetic shielding has been reported, studies combining these composites with both electromagnetic shielding and thermal conductivity properties are limited. Thus, this study aims to fabricate 3D graphene-CNT-SiC materials by self-assembling graphene oxide through liquid-phase reduction. SiC whiskers serve as the framework, and multi-walled carbon nanotubes act as the reinforcing connecting phase. Subsequently, the electromagnetic shielding and thermal conductivity performances of the 3D graphene-CNT-SiC materials were evaluated.

2 Experimental

2.1 Materials

Graphene oxide powder (GO, layer diameter <40 μm) was obtained from Baotailong Graphene New Material Company. SiC whiskers (average particle size: ~ 800 nm, $L/D \geqslant 20$) were purchased from Suzhou Sailong Nano New Materials Industry Co., Ltd. Hydroxylated multi-walled carbon nanotubes (CNTs, TF-CNTs-006H) were from Suzhou Tanfeng Graphene Technology Co., Ltd. All chemical reagents were obtained from commercial sources and used as received, without any additional purification steps.

2.2 Preparation of 3D graphene-CNT-SiC materials

GO powder was dispersed in deionized water and sonicated for 1 h to prepare GO aqueous solution (5 $mg \cdot mL^{-1}$). SiC whiskers were weighed at mass fractions of 0.5%, 1.0%, 2.0% and 5.0% relative to GO, then added to 100 mL of deionized water containing 1.0% Polyvinyl pyrrolidone (PVP) and sonicated for 2 h to prepare SiC whisker dispersion solutions. 0.1 g of hydroxylated multi-walled carbon nanotubes (CNTs) were dispersed in 100 mL of deionized water and sonicated for 1 h to prepare the CNT dispersion.

During ultrasonication, the dispersion of SiC

whiskers was slowly introduced into the CNTs dispersion, and sonicated for 2 h to achieve homogeneous dispersion and composite formation of CNTs and SiC whiskers. Subsequently, during ultrasonic treatment, the SiC/CNT dispersion was added to the graphene oxide dispersion and further sonicated for 1 h. Then, 0.5 g of ascorbic acid was added to the aforementioned solution, followed by sonication for 10 min. The mixture was subsequently reduced at 95 °C for 3 h in a water bath. After the reaction, the samples were washed with deionized water until pH became neutral, followed by freeze-drying for 48 h. The freeze-dried powder samples were then heat-treated in a tube furnace under Ar gas protection at 900 °C for 2 h. The composition of the samples is provided in Table 1.

2.3 Characterization

The microstructural morphology of the specimens was examined using a scanning electron microscope (Helios Nanolab 600i SEM). The crystal structures of the as-prepared materials were identified using a D/MAXRC XRD instrument equipped with a Cu-*K*α radiation source (40.0 kV, 40.0 mA). The chemical compositions of the samples were determined by XPS (Thermo Escalab 250Xi, USA). The specific surface area and pore size distribution of the synthesized materials were analyzed using Brunauer–Emmett–Teller (BET) measurements (Belsorp mini II, Japan). Electrical conductivity was assessed via the four-probe method (YAOS FM100GH). The electromagnetic parameters were evaluated using a waveguide method on an Agilent N5234A vector network analyzer. Circular test specimens, each with an inner diameter of 25.4 mm and a thickness of 1 mm, were fabricated for evaluating EMI shielding effectiveness and thermal conductivity. The thermal conductivity of the 3D graphene-CNT-SiC material was assessed using a laser flash analysis instrument (NETZSCH LFA 467). Each sample underwent 5 measurements, and subsequently, the average value was calculated. Thermal infrared imaging was conducted using a BY1515 heating platform set to temperature of 100 °C.

3 Results and discussion

3.1 Structure of the 3D graphene-CNT-SiC

Fig. 1 illustrates the microstructural morphology of 3D graphene-CNT-SiC materials with varying SiC contents. As shown in Fig. 1(a1-a3), a 3D porous structure is observed in all SiC-0% samples, with pore sizes ranging approximately from 2 to 5 μm.

In the SiC-0.5% sample (Fig. 1(b1-b3)), a distinct morphology of graphene sheets loaded with carbon nanotubes on the surface of porous graphene layers is observed. But no SiC whiskers are detected, possibly due to the low content of silicon carbide whiskers, which are enveloped by graphene sheets. As shown in Fig. 1(c1-c3) and Fig. 1(d1-d3), as the SiC content increased from 0.5% to 2.0%, SiC whiskers are prominently observed traversing through the three-dimensional graphene porous structure. As the SiC content increases from 2.0% to 5.0%, severe agglomeration of SiC whiskers occurs within the matrix material (Fig. 1e-2), which severely impedes the performance of the material.

The aforementioned results indicate that SiC whiskers can constitute the framework of 3D graphene-CNT-SiC materials. The SiC framework provides robust support for the three-dimensional porous structure of graphene, effectively preventing pore collapse.

To further characterize the microstructural morphology of the samples, TEM images of 3D graphene-CNT-SiC materials were recorded (Fig. 2). As depic-

Table 1 The compositions of 3D graphene-CNT-SiC materials

Sample	GO/g	CNT/g	SiC/mg	Mass percentage of SiC relative to GO/%
SiC-0%	5	1	0	0
SiC-0.5%	5	1	25	0.5%
SiC-1.0%	5	1	50	1.0%
SiC-2.0%	5	1	100	2.0%
SiC-5.0%	5	1	250	5.0%

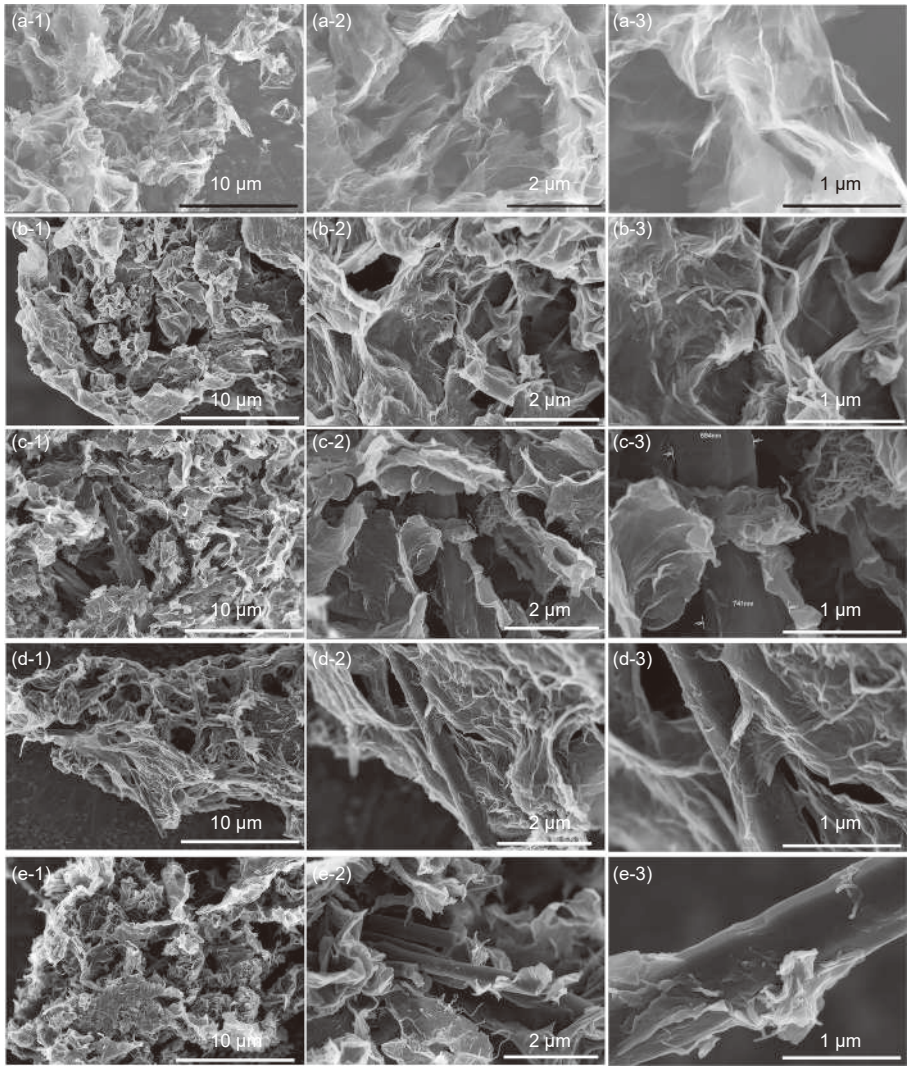

Fig. 1　SEM images of 3D graphene-CNT-SiC materials: (a) SiC-0%, (b) SiC-0.5%, (c) SiC-1.0%, (d) SiC-2.0%, (e) SiC-5.0%

ted in Fig. 2a, whisker-like SiC, curved CNTs and sheet-like graphene can be observed in the SiC-2.0% sample. By magnifying the area outlined by the yellow rectangle, it is clearly observed that the nanoscale CNTs attach to the surface of the SiC whiskers at one end, while the other end connects to the graphene sheets, thereby forming a leaf-like structure (Fig. 2b-2c). The SiC-5.0% sample exhibits a microstructural morphology similar to that of the SiC-2.0% sample, as shown inFig. 2e-g. This result indicates that the leaf-like structure connecting graphene and SiC whiskers by CNTs is commonly present in 3D graphene-CNT-SiC materials. This characteristic may further enhance the interfacial connection between SiC whiskers and graphene sheets as shown in Fig. 3.

The addition of CNTs can effectively reinforce the connection between SiC whiskers and graphene sheets, thereby enhancing the interlayer thermal conductivity of the material. Simultaneously, the 3D porous structure constructed by highly conductive graphene sheets facilitates the multiple emission and dissipation of electromagnetic waves within the hybrid material, thereby enhancing the EMI effect of the hybrid material. Consequently, the SiC framework and the 3D porous structure in 3D graphene-CNT-SiC materials provide a structural foundation for excellent thermal conductivity and electromagnetic shielding performance.

Fig. 4a presents the XRD patterns of 4 samples. As depicted in Fig. 4a, a wide diffraction peak at 26.3° can be seen, which corresponds to the (002) plane of reduced graphene oxide. This result confirms

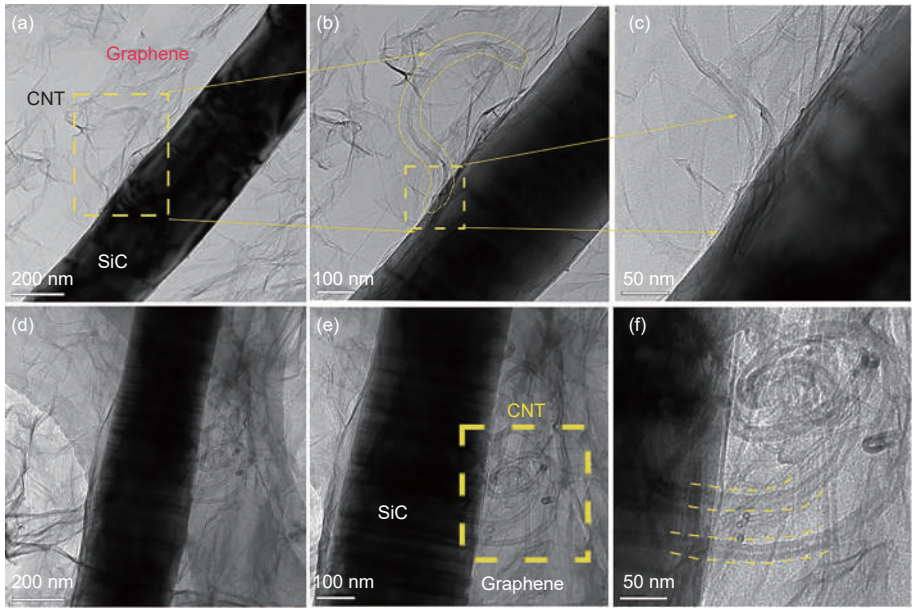

Fig. 2 TEM images of 3D graphene-CNT-SiC materials: (a, b, c) SiC-2.0%; (d, e, f) SiC-5.0%

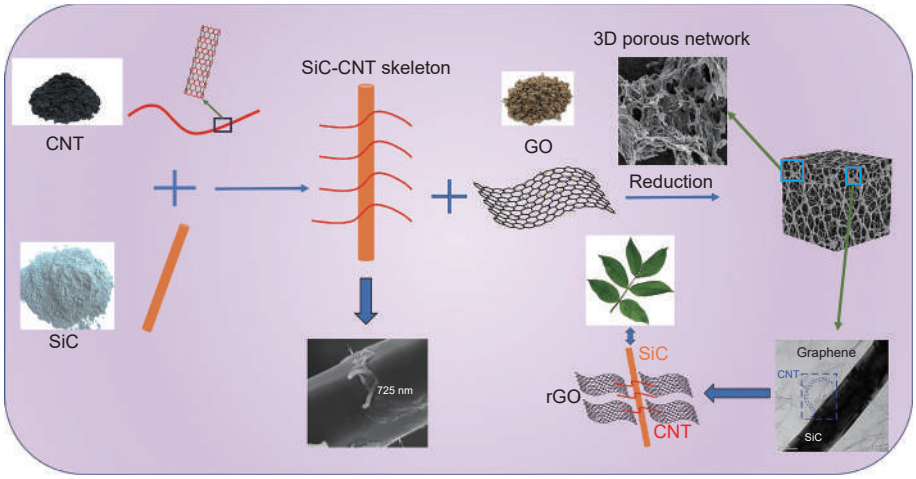

Fig. 3 Schematic illustration for the fabrication of 3D graphene-CNT-SiC materials

the successful reduction of GO. The prominent diffraction peaks at 35.7°, 42.9°, 60.1° and 72.0° can be indexed to the characteristic peaks of SiC, corresponding to the (0 1 5), (0 1 11), (0 1 20) and (2 0 5) crystal planes of β-SiC, respectively.

Fig. 4b-d present the XPS spectra of the 3D graphene-CNT-SiC (SiC-2.0%) sample. As can be seen in Fig. 4b, the XPS survey spectrum of the SiC-2.0% sample exhibits C 1s and Si 2p peaks. Fig. 4c-d show the peak fitting diagrams of the C 1s and Si 2p peaks, respectively. As shown in Fig. 4c, the C 1s spectrum of the SiC-2.0% sample reveals peaks corresponding to sp^2-hybridized carbon atoms (C=C at 284.5 eV), sp^3-hybridized carbon atoms (C—C at 284.8 eV), oxhydryl groups (C—OH at 285.8 eV), and carbonyl groups (C=O at 287.1 eV)[19,20], with contents of 20.86%, 69.31%, 7.42% and 2.41%, respectively. The results indicate that graphene oxide has been fully reduced, which contributes to the excellent thermal conductivity and dielectric loss performance of 3D graphene. As shown in Fig. 4d, the Si 2p spectrum of the SiC-2.0% sample only shows the Si-C peak (102.19 eV) with a content of 100%, indicating the presence of SiC in the hybrid material.

3.2 Pore size distribution

As illustrated in Fig. 5, the Brunauer–Emmett–Teller (BET) specific surface area and pore size distribution characteristics of the 3D graphene-CNT-SiC

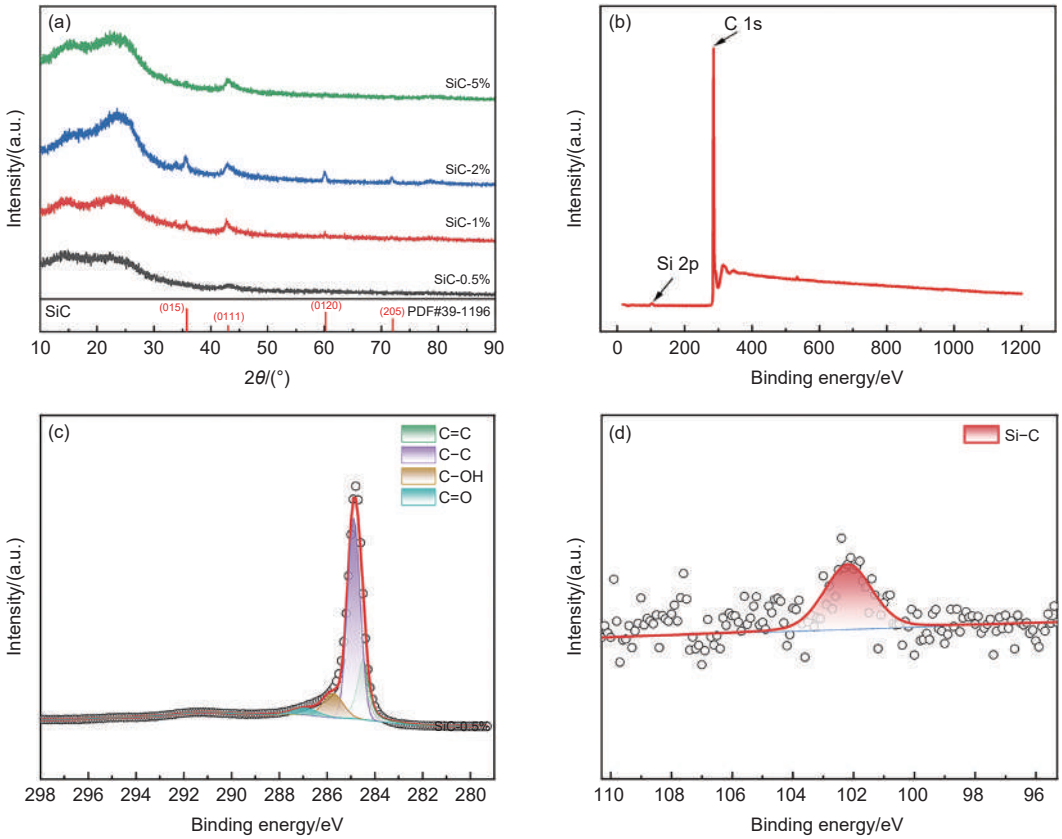

Fig. 4　(a) XRD patterns of 3D graphene-CNT-SiC materials. XPS spectra of the SiC-2.0%: (b) survey spectrum; (c) C 1s spectrum; (d) Si 2p spectrum

(0.5%, 1.0%, 2.0% and 5.0%) materials were investigated by nitrogen isothermal adsorption. Fig. 5a-d exhibit the nitrogen adsorption and desorption isotherms of the samples. As shown in Fig. 5a-d, within the range of $0.45 < p/p_0 < 1.0$, all samples exhibit elongated H3 hysteresis loops. The sample of SiC-2.0% shows particularly pronounced features compared to the others. Fig. 5a-d indicate that the isotherms of the 3D graphene-CNT-SiC materials exhibit properties of type IV according to the IUPAC classification, which is indicative of a mesoporous structure (2–50 nm)[21].

The pore size distribution curves of the 3D graphene-CNT-SiC samples are shown in Fig. 5e-h. As illustrated in Fig. 5e-h, it can be observed that the pore size diameters of the samples are predominantly in the range of 2–3 nm and 20–50 nm. As the SiC whisker content increases from 0.5% to 5.0%, there is a significant increase in the number of pores with diameters of 2–3 nm in 3D graphene-CNT-SiC, while the number of pores with diameters of 20–50 nm markedly decreases. As shown in Fig. 6, with the increase in SiC content, the specific surface area of the samples increases from 16.78 to 60.10 $m^2 \cdot g^{-1}$, and the pore volume increases from 0.06 to 0.25 $cm^3 \cdot g^{-1}$, which is consistent with the literature reports[22]. The increase in specific surface area and pore volume may be attributed to the significant increase in the number of pores with diameters of 2–3 nm. This result indicates that the SiC content can affect the pore structure parameters of the hybrid material during the self-assembly process of GO nanosheets into a 3D porous structure. Larger specific surface area and pore volume are evident in the samples with an increased SiC content. Therefore, the SiC content in 3D graphene-CNT-SiC can adjust the characteristics of pore structure, which can significantly influence the electromagnetic shielding performance of the material.

The electrical conductivity of 3D graphene-CNT-SiC materials is shown in Fig. 7. The SiC-0% sample exhibits the highest electrical conductivity, with a value of 140.64 S m^{-1}. This result indicates that 3D

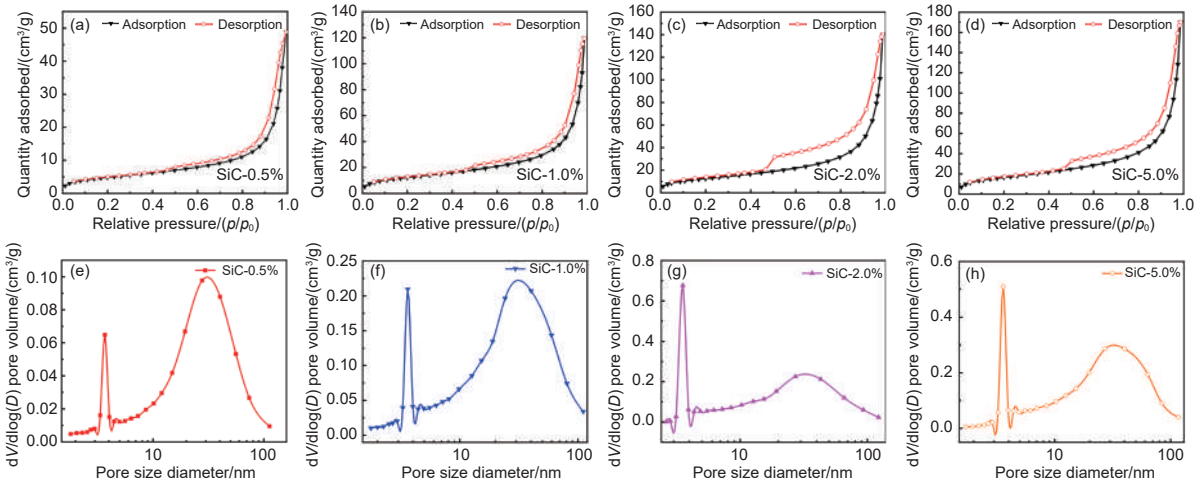

Fig. 5 (a-d) Nitrogen adsorption/desorption isotherms and (e-h) pore size distribution curves of 3D graphene-CNT-SiC materials: (a, e) SiC-0.5%; (b, f) SiC-1.0%; (c, g) SiC-2.0% ; (d, h) SiC-5.0%

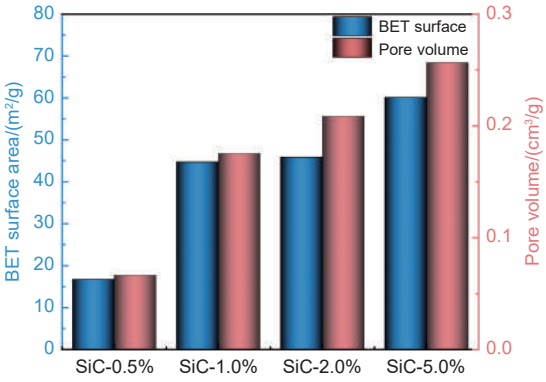

Fig. 6 BET surface area and pore volume of 3D graphene-CNT-SiC materials

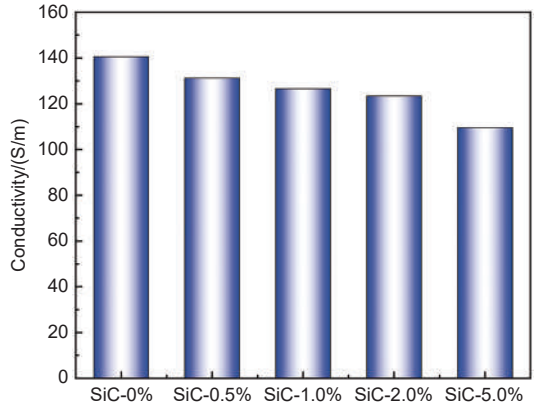

Fig. 7 Electrical conductivity of 3D graphene-CNT-SiC materials

graphene has an excellent conductive network, which is advantageous for both the reflection and absorption of electromagnetic waves[17]. As the SiC content increases from 0.5% to 5.0%, the electrical conductivity of the 3D graphene-CNT-SiC materials gradually decreases from 131.22 to 109.67 S m^{-1}. This decline is primarily attributed to the non-conductive nature of SiC whiskers[22]. The combination of graphene and SiC, each with unique electrical conductivity and permittivity, can lead to charge buildup and polarization at their interfaces, thereby greatly improving the absorption of electromagnetic waves[17].

3.3 EMI shielding performance

Fig. 8 shows EMI SE_A, SE_R and SE_T curves and bar graph of the average SE_T of 3D graphene-CNT-SiC materials in the X band (8–12 GHz). In the EMI shielding evaluation, a fraction of the incident electromagnetic waves undergoes initial reflection upon encountering the surface of the specimen, while another portion is absorbed, leaving behind the remaining waves to transmit through the sample. In general, the overall shielding effectiveness (SE_T) can be approximately estimated as the aggregate of the absorption shielding effectiveness (SE_A) and the reflection shielding effectiveness (SE_R)[16].

We observe that compared to SE_R, SE_A is the primary contributor to the SE_T value (Fig. 8d). This finding can be mainly attributed to the presence of a 3D porous structure in the 3D graphene-CNT-SiC sample (Fig. 1). The conductive graphene network in the highly developed 3D porous structure improves the impedance matching at the foam/air interface. Accordingly, the EMI shielding performances are enhanced by reducing back reflection and absorbing

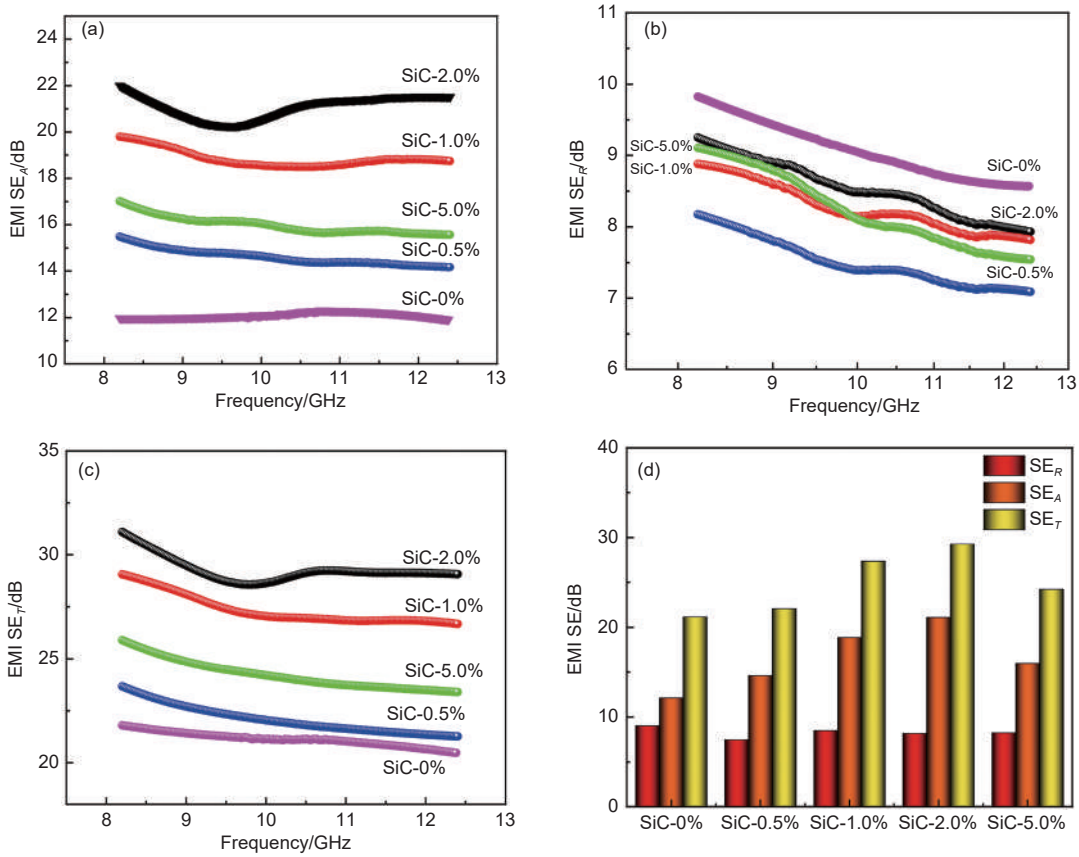

Fig. 8　(a) EMI SE$_A$; (b) EMI SE$_R$; (c) EMI SE$_T$ and (d) the average SE of 3D graphene-CNT-SiC materials

more radiation through conductive dissipation and multiple scattering[23,24]. As the electromagnetic wave permeates the interior of the porous material, a portion is absorbed through the conduction losses of graphene, while another fraction undergoes multiple reflections within the 3D graphene skeleton (Fig. 9), which increases the SE$_A$ of the 3D graphene-CNT-SiC[18]. As illustrated in Fig. 8b, the SE$_R$ curve for the SiC-0% is higher than those of the other samples, which may be attributed to its high electrical conductivity. The SE$_R$ curves for the samples are quite similar and higher than that of the SiC-0.5% sample. This result is attributed to the comparable impedance mismatch between air and the samples for the SiC-1.0%, SiC-2.0% and SiC-5.0% samples, which is consistent with the findings reported in the literature[17,25].

As depicted in Fig. 8d, the SiC-0.5% sample exhibits a SE$_T$ of 20.07 dB. The SiC-1.0% sample demonstrates an enhanced SE$_T$ value of 27.34 dB, and this improvement is further augmented to 29.26 dB for the SiC-2.0% sample. This result indicates a significant enhancement in the electromagnetic shielding performance of the samples with increasing SiC content. This phenomenon is primarily ascribed to the enhancement in pore structure parameters and the augmentation of heterogeneous interfaces in 3D graphene-CNT-SiC with the elevation of SiC content. As illustrated in Fig. 5, the specific surface area and pore volume of samples both increase with the significant increase in the number of pores with diameters of 2–3 nm as the SiC content rises from 0.5% to 2.0%. The smaller pore size and larger specific surface area contribute to increasing the number of solid/air interfaces[26,27], thereby greatly enhancing the multiple reflections of electromagnetic waves within the material, resulting in significant attenuation of incident electromagnetic waves (Fig. 9)[26]. Meanwhile, the integration of carbon (graphene or CNT) and SiC, which possess different electrical conductivities and permittivities, can lead to charge buildup and polarization at their diverse interfaces. This phenomenon greatly improves the absorption of electromagnetic waves[17,28].

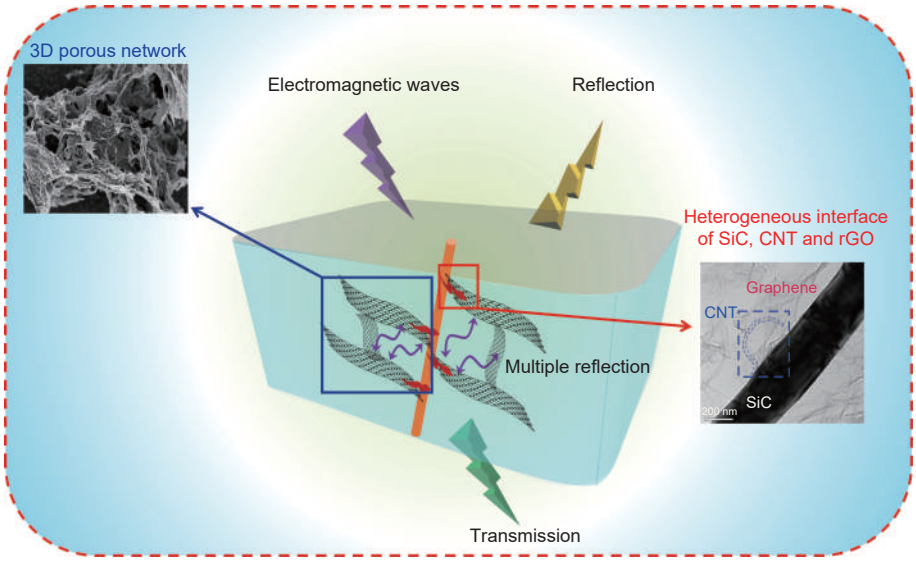

Fig. 9 Schematic representation of the EMI shielding of 3D graphene-CNT-SiC materials

With the increase of SiC content, the increase in the number of heterogeneous interfaces facilitates enhancing interfacial and dipole polarization, thereby amplifying polarization losses (Fig. 9), which agrees with the conclusions reported in the literature[17,22].

Compared with the SiC-2.0% sample, the SiC-5.0% sample exhibits a slightly lower SE_T value (24.21 dB). This observation could potentially be attributed to the agglomeration of excessive SiC whiskers as shown in Fig. 1e-2, which leads to a sharp decrease in the number of heterogeneous interfaces. Consequently, this result may significantly diminish the synergistic polarization loss of 3D graphene-CNT-SiC for electromagnetic wave absorption.

In general, a material exhibiting a total shielding effectiveness of 20 dB, signifying that it blocks 99% of the incoming electromagnetic waves, is deemed sufficient for meeting the requirements of most commercial applications[25,29]. As depicted in Fig. 8, the total shielding effectiveness (SE_T) values for all samples exceed 20 dB, indicating that 3D graphene-CNT-SiC materials represent lightweight materials with excellent electromagnetic shielding properties.

3.4 Thermal conductivity

In addition to electromagnetic shielding performance, the thermal management properties of 3D graphene-CNT-SiC materials were also investigated. The 3D graphene-CNT-SiC samples were positioned on a heating platform maintained at a steady temperature of 100 °C, and thermal infrared images were obtained using an infrared camera. As shown in Fig. 10a-d and Fig. S2, the infrared thermography images of 3D graphene-CNT-SiC materials with varying concentrations (0%, 0.5%, 1.0%, 2.0% and 5.0%) were recorded. Fig. 10e shows the temperature difference between the hot center and the edge of 3D graphene-CNT-SiC materials during infrared thermal imaging tests. Table 2 summarizes the temperature differentials between the center and edges of the samples. It is well known that the utilization of materials with high thermal conductivity leads to minimal temperature differentials between the center and edges of the material. This phenomenon arises from the exceptional thermal conductivity of the materials, which rapidly dissipates heat from the heat source to the surroundings, enabling rapid thermal homogenization. As shown in Table 2, during the infrared thermal imaging tests, the temperature differentials between the center and edges of the 3D graphene-CNT-SiC (0%, 0.5%, 1.0%, 2.0% and 5.0%) samples were 23, 18.6, 12.6, 4.9 and 10.8 °C, respectively. The SiC-2.0% sample exhibited a notably lower temperature differential, indicating the best heat dissipation ability among the samples.

The thermal conductivity of the 3D graphene-CNT-SiC (0.5%, 1.0%, 2.0% and 5.0%) samples is

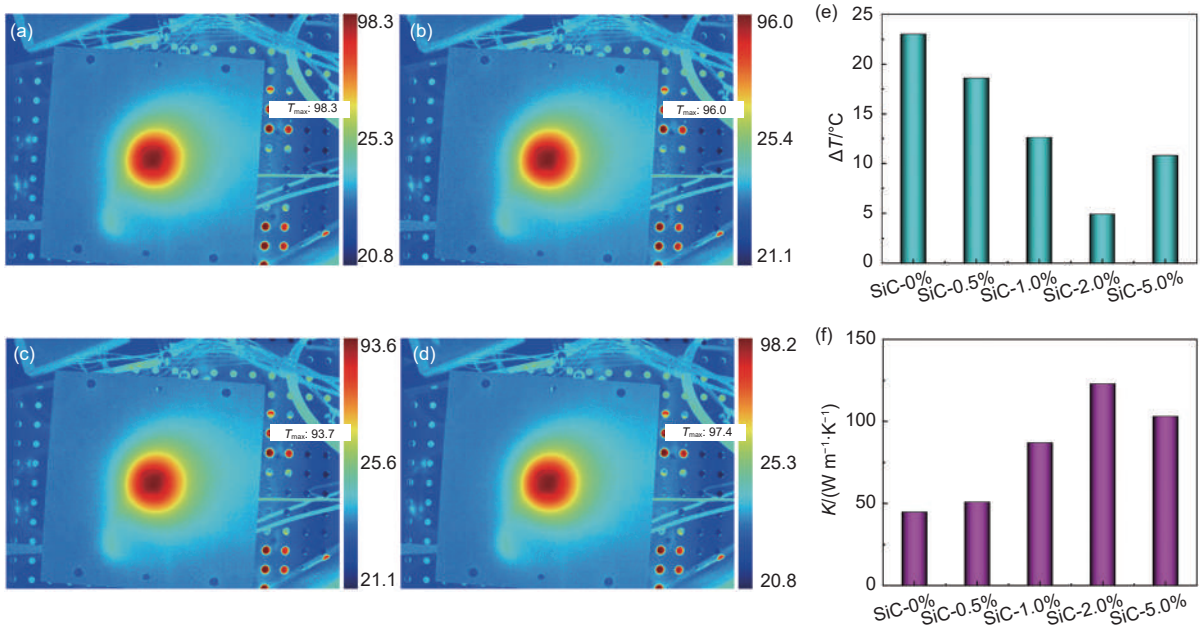

Fig. 10　Infrared thermal images of (a) SiC-0.5%, (b) SiC-1.0%, (c) SiC-2.0% and (d) SiC-5.0%. (e) Temperature difference between the center and the edge of heat source of 3D graphene-CNT-SiC materials. (f) Thermal conductivity of 3D graphene-CNT-SiC materials

Table 2　Thermal conductivity of 3D graphene-CNT-SiC materials and the temperature differentials between the center and the edge of the samples

Sample	Thermal conductivity/ ($W \cdot m^{-1} \cdot K^{-1}$)	ΔT /°C
SiC-0%	45	23.0
SiC-0.5%	51	18.6
SiC-1.0%	87	12.6
SiC-2.0%	123	4.9
SiC-5.0%	103	10.8

provided in Fig. 10f and Table 2. The thermal conductivity of the 3D graphene-CNT-SiC (0%, 0.5%, 1.0%, 2.0% and 5.0%) samples are 45, 51, 87, 123 and 103 $W \cdot m^{-1} \cdot K^{-1}$, respectively. The SiC-2.0% sample demonstrated the highest thermal conductivity, consistent with the results from infrared thermal imaging tests.

The exceptional thermal conductivity of the 3D graphene-CNT-SiC (2.0%) sample can be attributed to two primary factors: (1) The high-temperature thermal annealing process heals the defects of GO. In graphene's heat conduction, phonon diffusion plays a pivotal role, a phenomenon arising from the lattice vibrations within its covalent sp^2 bonding framework[30]. However, the presence of defects and grain boundaries within graphene sheets introduces thermal resistance, significantly impeding phonon transport through scattering mechanisms[30]. In this work, the 3D graphene-CNT-SiC (2.0%) underwent high-temperature thermal annealing, facilitating the further repair of oxidized graphene crystal defects and reducing grain boundaries. This process contributed to the exceptional thermal conductivity of the samples. (2) The branch-like structure of SiC-CNT enhances interlayer thermal conductivity in graphene. Unlike the in-plane direction, where phonons can freely propagate within a single layer, phonons in the vertical direction must traverse from one layer to another[18]. Therefore, overcoming the high interface thermal resistance between graphene sheets is necessary. As shown in Fig. 2 and Fig. 9, the use of high thermal conductivity SiC whiskers as a longitudinal thermal framework, reinforces the connection between graphene layers by CNTs and exploits the advantageous high thermal conductivity of SiC to establish longitudinal heat flow pathways. This approach enhances the thermal conductivity of the 3D graphene-CNT-SiC material. Table 3 provides the results of the electromagnetic shielding and thermal conductivity performance of 3D graphene-CNT-SiC compared with other graphene or SiC-based materials reported in recent literature.

Table 3 Performance comparison between 3D graphene-CNT-SiC materials and graphene or SiC-based composites in literatures

Materials	Thickness/mm	EMI SE/dB	Thermal conductivity/(W· m^{-1}·K^{-1})	Ref.
G/PDMS	1.0	20.0		[31]
GA/PI	2.0	28.0		[32]
CNT/G	1.6	38.4		[33]
G-SiCNW	1.2	32.5	2.1	[34]
SrGO foam	2.0	25.3		[17]
Graphene/carbon fiber	2.0	73.0	1.7	[35]
C/(PyC-SiC)n	2.0	37.1	6.0	[36]
GF@SiCNW	2.0	36.0	322.0	[37]
SiCNWs/SiC	2.8	38.3	13.8	[38]
3D graphene-CNT-SiC	1.0	29.3	123.0	This work

Notes: G: graphene; PDMS: poly(dimethyl siloxane), GA: graphene aerogel, PI: polyimide, SiCNW: SiC nanowires, PyC: pyrocarbon, GF: graphite flake

4 Conclusions

A series of 3D graphene-CNT-SiC materials with different SiC contents were successfully synthesized by liquid-phase reduction. The microstructure, pore size distribution, electromagnetic shielding performance and thermal conductivity of the samples were characterized. This study revealed that SiC whiskers penetrated the 3D porous structure of graphene, providing structural support. The 3D porous structure and multiphase heterogeneous interfaces in the 3D graphene-CNT-SiC materials were found to enhance the electromagnetic shielding performance of the samples. The branch-like morphology of SiC-CNT enabled longitudinal thermal conduction pathways, significantly enhancing the thermal conductivity of the 3D graphene-CNT-SiC materials. At 2.0% SiC content, the sample exhibited outstanding thermal conductivity and electromagnetic shielding performance. The thermal conductivity of 3D graphene-CNT-SiC (2.0%) is 123 $W\cdot m^{-1}\cdot K^{-1}$. In the X-band frequency range, the electromagnetic interference shielding effectiveness (EMI SE_T) of the hybrid materials reached 29.3 dB. We believe that 3D graphene-CNT-SiC may open a new avenue for designing dual-functional hybrid material with high thermal conductivity and electromagnetic shielding performance, promoting their use in various applications.

Acknowledgements

This work was supported by the Basic Scientific Research Foundation of Higher Educational Institutions in Heilongjiang Province 2022-KYYWF-0528.

References

[1] Liu D, Yang Z, Zhang Y, et al. Tailoring aligned and densified carbon nanotube@graphene coaxial yarn for 3D thermally conductive networks[J]. Carbon, 2023, 208: 322-329.

[2] Rangarajan S, Schiffres S N, Sammakia B. A review of recent developments in “on-chip” embedded cooling technologies for heterogeneous integrated applications[J]. Engineering, 2023, 26: 185-197.

[3] Salmon F, Ghadim H B, Godin A, et al. Optimizing performance for cooling electronic components using innovative heterogeneous materials[J]. Applied Energy, 2024, 362: 122983.

[4] Wen Y, Chen C, Ye Y, et al. Advances on thermally conductive epoxy-based composites as electronic packaging underfill materials-a review[J]. Advanced Materials, 2022, 34(52): e2201023.

[5] Zhao C, Li Y, Liu Y, et al. A critical review of the preparation strategies of thermally conductive and electrically insulating polymeric materials and their applications in heat dissipation of electronic devices[J]. Advanced Composites and Hybrid Materials, 2022, 6(1): 1-26.

[6] Zhang Y, Ruan K, Gu J. Flexible sandwich-structured electromagnetic interference shielding nanocomposite films with excellent thermal conductivities[J]. Small, 2021, 17(42): e2101951.

[7] Geim A K, Novoselov K S. The rise of graphene[J]. Nature Materials, 2007, 6(3): 183-191.

[8] Novoselov K S, Fal'ko V I, Colombo L, et al. A roadmap for graphene[J]. Nature, 2012, 490(7419): 192-200.

[9] Yang W, Yan L, Jiang B, et al. Crumpled nitrogen-doped porous carbon nanosheets derived from petroleum pitch for high-performance and flexible electromagnetic wave absorption[J]. Iindustrial & Engineering Chemistry Research, 2022, 61(7): 2799-2808.

[10] Yang W, Bai H X, Jiang B, et al. Flexible and densified graphene/waterborne polyurethane composite film with thermal conducting property for high performance electromagnetic interference shielding[J]. Nano Research, 2022, 15(11): 9926-

9935.

[11] Kim H S, Kim Y W. Thermal conductivity of liquid-phase sintered silicon carbide ceramics: A review[J]. Journal of the European Ceramic Society, 2023, 43(9): 3855-3874.

[12] Yao Y, Zeng X, Pan G, et al. Interfacial engineering of silicon carbide nanowire/cellulose microcrystal paper toward high thermal conductivity[J]. ACS Applied Materials & Interfaces, 2016, 8(45): 31248-31255.

[13] Cheng Z, Liang J, Kawamura K, et al. High thermal conductivity in wafer-scale cubic silicon carbide crystals[J]. Nature Communications, 2022, 13(1): 7201.

[14] Chen Q, Wang H, Gao H, et al. Effects of porous silicon carbide supports prepared from pyrolyzed precursors on the thermal conductivity and energy storage properties of paraffin-based composite phase change materials[J]. Journal of Energy Storage, 2022, 56: 106046.

[15] Shi A, Zhang X, Meng J, et al. Waffle-inspired thermal conductive silicone rubber composites with excellent electromagnetic shielding performance based on three-dimensional filler networks[J]. Materials Letters, 2023, 350: 134940.

[16] Xie A, Zhang B, Ge Y, et al. The microstructure and electromagnetic interference shielding effectiveness of C/C composite surfaces modified by SiC nanoribbons@vertically oriented graphene[J]. Journal of Materials Research and Technology, 2023, 25: 4833-4841.

[17] He X, Feng L, Zhang Z, et al. High-performance multifunctional carbon-silicon carbide composites with strengthened reduced graphene oxide[J]. ACS Nano, 2021, 15(2): 2880-2892.

[18] Zhao X, Wu W, Drummer D, et al. SiC nanowires bridged graphene aerogels with a vertically aligned structure for highly thermal conductive epoxy resin composites and their mechanism[J]. ACS Applied Electronic Materials, 2023, 5(5): 2548-2557.

[19] Shen Y, Jing T, Ren W, et al. Chemical and thermal reduction of graphene oxide and its electrically conductive polylactic acid nanocomposites[J]. Composites Science and Technology, 2012, 72(12): 1430-1435.

[20] Vallés C, David Núñez J, Benito A M, et al. Flexible conductive graphene paper obtained by direct and gentle annealing of graphene oxide paper[J]. Carbon, 2012, 50(3): 835-844.

[21] Tang X, Liu Z H, Zhang C, et al. Synthesis and capacitive property of hierarchical hollow manganese oxide nanospheres with large specific surface area[J]. Journal of Power Sources , 2009, 193(2): 939-943.

[22] Li J, Qi Y Q, Zhao S X, et al. RGO@SiC porous films based multilayer electromagnetic shields[J]. New Carbon Materals, 2024, 39: 1-11.

[23] Gupta S, Tai N H. Carbon materials and their composites for electromagnetic interference shielding effectiveness in X-band[J]. Carbon, 2019, 152: 159-187.

[24] Xia Y, Gao W, Gao C. A review on graphene-based electro[J]. Advanced Functional Materials , 2022, 32(42): 2204591.

[25] Wei Y, Liu Y S, Zhao M X, et al. Effect of heat treatment temperature on microstructure and electromagnetic shielding properties of graphene/SiBCN composites[J]. Journal of Materials Science & Technology, 2019, 35(12): 2897-2905.

[26] Dai Z, Wei Y, Hu C, et al. Effects of pore structure on wide-frequency electromagnetic interference shielding performance of carbonized wood[J]. Composites Communications, 2023, 38: 101501.

[27] Ma L, Hamidinejad M, Wei L, et al. Absorption-dominant EMI shielding polymer composite foams: microstructure and geometry optimization[J]. Materials Today Physics, 2023, 30: 100940.

[28] Liang L, Yao C, Yan X, et al. High-efficiency electromagnetic interference shielding capability of magnetic $Ti_3C_2T_x$ MXene/CNT composite film[J]. Journal of Materials Chemistry A, 2021, 9(43): 24560-24570.

[29] Yang Y, Gupta M C, Dudley K L, et al. Novel carbon nanotube-polystyrene foam composites for electromagnetic interference shielding[J]. Nano Letters, 2005, 5(11): 2131-4.

[30] Peng L, Xu Z, Liu Z, et al. Ultrahigh thermal conductive yet superflexible graphene films[J]. Advanced Materials, 2017, 29(27): 1700589.

[31] Chen Z, Xu C, Ma C, et al. Lightweight and flexible graphene foam composites for high-performance electromagnetic interference shielding[J]. Advanced Materials, 2013, 25(9): 1296-300.

[32] Yu Z, Dai T, Yuan S, et al. Electromagnetic interference shielding performance of anisotropic polyimide/graphene composite aerogels[J]. ACS Applied Materials & Interfaces, 2020, 12(27): 30990-31001.

[33] Song Q, Ye F, Yin X, et al. Carbon nanotube-multilayered graphene edge plane core-shell hybrid foams for ultrahigh-performance electromagnetic-interference shielding[J]. Advanced Materials, 2017, 29(31): 1701583.

[34] Liang C, Hamidinejad M, Ma L, et al. Lightweight and flexible graphene/SiC-nanowires/ poly(vinylidene fluoride) composites for electromagnetic interference shielding and thermal management[J]. Carbon, 2020, 156: 58-66.

[35] Li X, Xu T, Cao W, et al. Graphene/carbon fiber network constructed by co-carbonization strategy for functional integrated polyimide composites with enhanced electromagnetic shielding and thermal conductive properties[J]. Chemical Engineering Journal , 2023, 464: 142595.

[36] Tian X, Li H, Yang L, et al. Electromagnetic shielding and thermal conductive properties of SiC nanowires reinforced C/(PyC-SiC)*n* composites[J]. Ceramics International, 2021, 47(1): 590-597.

[37] Zhang X, Zhang B, Wei Z, et al. SiC skeleton-reinforced highly oriented graphite with good thermophysical and electromagnetic shielding properties[J]. Journal of the American Ceramic Society, 2024, 107(6): 3945-3958.

[38] Hou W, Feng T, Shi X, et al. Multifunctional nanocomposites integrate electromagnetic shielding, thermal, mechanical, and wear resistance properties[J]. Journal of the American Ceramic Society, 2023, 106(6): 3351-3358.